

Anomalous metals: From “failed superconductor” to “failed insulator”

Xinyang Zhang^{a,b,1}, Alexander Palevski^c, and Aharon Kapitulnik^{a,b,d}

^aGeballe Laboratory for Advanced Materials, Stanford University, Stanford, CA 94305, USA; ^bDepartment of Applied Physics, Stanford University, Stanford, CA 94305, USA; ^cSchool of Physics and Astronomy, Raymond and Beverly Sackler Faculty of Exact Sciences, Tel Aviv University, Tel Aviv 6997801, Israel; ^dDepartment of Physics, Stanford University, Stanford, CA 94305, USA

This manuscript was compiled on June 8, 2022

1 **Resistivity saturation is found on both superconducting and insulating sides of an “avoided” magnetic-field-tuned superconductor-to-insulator transition (H-SIT) in a two-dimensional In/InO_x composite, 2 where the anomalous metallic behavior cuts off conductivity or resistivity divergence in the zero-temperature limit. The granular morphology of the material implies a system of Josephson junctions (JJ) 3 with a broad distribution of Josephson coupling E_J and charging energy E_C , with an H-SIT determined by the competition between 4 E_J and E_C . By virtue of self-duality across the true H-SIT, we invoke 5 macroscopic quantum tunneling effects to explain the temperature- 6 independent resistance where the “failed superconductor” side is a 7 consequence of phase fluctuations and the “failed insulator” side 8 results from charge fluctuations. While true self-duality is lost in the 9 avoided transition, its vestiges are argued to persist, owing to the 10 incipient duality of the percolative nature of the dissipative path in 11 the underlying random JJ system.**

anomalous metals | quantum fluctuations | self-duality | Josephson junction array

1 **A**n increasing number of recent experiments on disordered superconducting films, initially searching for a 2 superconductor-to-insulator transition (SIT), end up instead with an “avoided” transition, where scaling about a putative 3 zero-temperature quantum critical point fails in the limit $T \rightarrow 0$, giving way to a phase characterized by a resistance 4 that levels off to a constant value independent of temperature 5 (1–8). This “anomalous metallic state” (AMS) seems to exhibit 6 electronic properties that cannot be understood on the basis 7 of the standard paradigms for transport in disordered two-dimensional (2d) metals (for a recent review see (9)). While 8 extensive efforts have been devoted to understanding AMS on the 9 superconducting side, termed a “failed superconductor,” 10 (9) and its transition to a “true” superconducting state (10), the 11 complementary leveling of resistance on the insulating side 12 of the same avoided SIT is often overlooked. Here, an initial 13 resistivity divergence trend for $T \rightarrow 0$ is replaced with distinct 14 saturation, exhibiting resistivity values that can be orders 15 of magnitude higher than quantum of resistance for Cooper 16 pairs $R_Q = h/e^2 \sim 6.45 \text{ k}\Omega$. This ubiquitous behavior of a 17 “failed insulator” can be found in studies of ultrathin granular 18 metal films (11), amorphous metal-insulator films (3, 12), and 19 Josephson junction (JJ) arrays (13).

20 In this paper we propose a unified phenomenology for the 21 emergence of anomalous metallic states from an avoided SIT in 22 disordered superconducting films. Focusing on the magnetic-field 23 tuned SIT (H-SIT) in strongly granular system of In-on-InO_x 24 composites, we show that vestiges of the self-duality observed 25 in a true H-SIT (14, 15) are still pronounced in the AMS on *both* 26 sides of the avoided-H-SIT (8), including the

resistance saturation. Bearing in mind that from its nature, the critical point of any SIT yields an anomalous metal, we propose that the broadening of the metallic phase on both sides of the H-SIT has the same origin modulo the dual relation between phase of the order parameter (or vortices) and charge (both cooper-pairs and single electrons). Specifically, we argue that the low-temperature resistance can be interpreted as a sum of a temperature-dependent activation term and a temperature-independent term associated with quantum fluctuations leading to macroscopic quantum tunneling (MQT) of the phase and/or the charge. On the superconducting side, a superconductor-to-quantum-metal transition (SQMT) appears with the destruction of global phase coherence (9, 16, 17), while on the insulating side quantum charge fluctuations prevent the establishment of a Coulomb-blockade-driven insulating state (13, 18, 19) driving a quantum-metal-to-insulator transition (QMIT).

The robustness of the anomalous metallic phase in the In/InO_x system (8) further enforces these expanded observations, while strongly contending interpretations solely based on non-equilibrium effects and responses to extrinsic effects of the electronic system (20) (see also Methods section.) At the same time, the temperature-independent term associated with MQT depends delicately on the details of the distribution of grains and junctions, which may be controlled by external effects leading to different saturation value of the resistance,

Significance Statement

A ubiquitous observation of robust metallic ground states arising from “failed superconductors” has attracted much attention in recent years because it presents a fundamental challenge to the standard theory of electron fluids. Meanwhile, observations of analogous metallic phases arising from “failed insulators” are often overlooked in analysis of similar data. Aiming to reconcile observations of both regimes in strongly granular In/InO_x two-dimensional films, we propose a unified understanding of these seemingly different anomalous metallic phases by drawing connections to resistive-capacitive-shunted Josephson junction arrays. Effects of quantum phase/charge fluctuations and macroscopic quantum tunneling are invoked to understand the anomalous metallic phase, thus advancing fundamental understandings of metals beyond the standard Fermi liquid theory.

X.Z., A.P., and A.K. designed the experiments. X.Z. grew the samples and performed measurements. X.Z. and A.K. analyzed the data and wrote the manuscript.

The authors declare no competing financial or non-financial interests.

¹To whom correspondence should be addressed. E-mail: xinyangz@stanford.edu

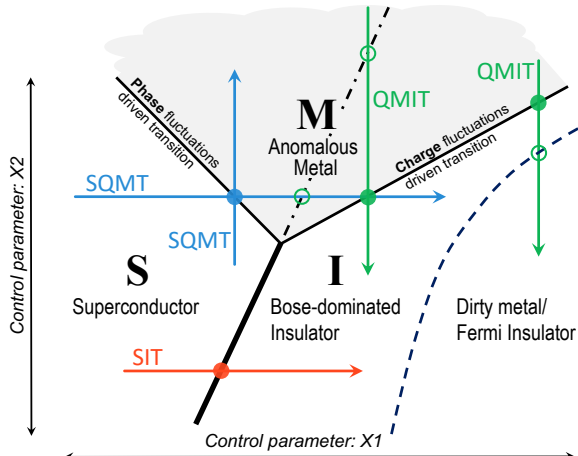


Fig. 1. Zero-temperature phase diagram of a 2D granular superconductor with two controlling parameters. In the present study, X_1 =magnetic field and X_2 =inter-grain coupling. Shaded area represents the region in parameter space where anomalous metal appears. Thick solid line represents a true H-SIT (Ref. (15)) while the other solid lines represent the transition from a superconductor to a quantum anomalous metal (SQMT) and from quantum anomalous metal to an insulator (QMIT). Dashed lines represent crossovers from a Bose dominated system, where superconducting In islands provide the source of pairing, to a normal-electrons insulator. Dash-dotted line represents the crossover from phase to charge dominated quantum anomalous metal state. Full circles represent a quantum critical point for a particular realization of the control parameters, while an open circle is a crossover point. See Discussion section for further explanations.

emphasizing its non-universal value in the anomalous metal regime. This in turn leads us to propose the phase diagram of Fig. 1 and suggest a unified understanding of anomalous metallic states in disordered superconducting films. Excluding the regime where pairs are no longer present, this phase diagram has strong resemblance to that of two-dimensional electron gas about half-filled Landau levels (21).

Whether samples are inherently inhomogeneous such as arrays of Josephson-junctions (JJ), or morphologically uniform such as amorphous films, superconducting pairing interaction tends to “amplify” mesoscopic fluctuations of the disorder and its associated Coulomb interaction, resulting in an effective granular morphology (22–25). Such puddle morphology was also argued to be a consequence of the competition between the local potential of randomly distributed charged impurities and screening by holes or by strongly bound Cooper pairs, yielding a similar phase diagram to our Fig. 1 (26). Therefore, it is reasonable to assume that the superconducting transition in 2d disordered metallic films is dominated by phase fluctuations (16, 17, 27) and the material can be modeled as superconducting grains embedded in a tunable intergrain coupling matrix. Here, we emphasize the truly two-dimensional granular morphology of our indium-on-indium oxide (In/In_x) system as shown in Fig. 2, which will be a key to our understanding of the data.

While local pair amplitude fluctuations depend on the grain size (29), global superconductivity is achieved via the establishment of a percolating path of phase coherence (30–33) through Josephson coupling of pairs of adjacent grains. For a given pair $\{ij\}$, E_J^{ij} is a function of the local gaps Δ_i and Δ_j and the intergrain normal-state resistance R_n^{ij} . However, the granular nature of 2d disordered films also requires that we

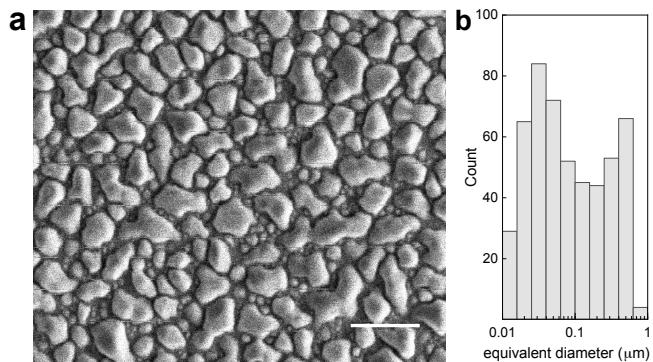


Fig. 2. Morphology of the In/InO_x system. a) Scanning electron microscopy image of the In/InO_x sample. Bright grains are metallic indium islands, while dark background is a uniform underlying layer of weakly-insulating amorphous InO_x . Note the broad distribution of grain sizes including the interstitial ones. Scale bar at lower right corner indicates $1\mu\text{m}$. b) Distribution of grain size. Note the two broad peaks at $\sim 0.03\mu\text{m}$ and $\sim 0.5\mu\text{m}$. See supplementary information for details in our image analysis (28).

consider the capacitance (both intergrain and self) involved and the associated charging energy E_C^{ij} which is a function of the local density at the grains n_i and n_j , and the dielectric constant of the intergrain material χ_n^{ij} . An insulating phase is the result of Coulomb blockade which prevent Cooper-pairs tunneling between adjacent grains. For a granular film with typical Josephson energy E_J and charging energy E_C , the ratio $\gamma \equiv E_J/E_C$ determines the occurrence of SIT (19, 34, 35). Besides the initial film morphology, other external parameters such as an applied magnetic field or carrier density modulation through an applied gate can be used to control γ .

Results

In Fig. 3, we plot temperature dependence of resistivity in varying perpendicular magnetic fields across three annealing stages S0, S1, and S2 of the same initial sample. Low-temperature annealing ($< 50^\circ\text{C}$) is well-known (36) to irreversibly reduce sample resistance yet maintain an amorphous nature of the underlying InO_x , thus altering the dielectric response in the poorly conducting matrix that couples superconducting grains. We restrict the range of magnetic field in this analysis to under 600 Oe to ensure robust superconductivity within the single grain (15).

Annealing stage S0 shows the most salient signatures of resistivity saturation on the insulating side of an “avoided” SIT. In zero field as temperature is lowered, resistivity decreases and saturates at around $6.2\text{ k}\Omega/\square$ as a failed superconductor. A magnetic field as low as 30 Oe flips temperature coefficient of resistance (TCR) to negative as in an insulator. However, the resistivity upturn gives way to saturation at around 0.2 K, eventually settling at a finite value as $T \rightarrow 0$. In higher fields the features are qualitatively similar, until at 600 Oe where resistivity strongly diverges and no saturation is found above our base temperature. In a broad range of magnetic field, we identify an insulator where resistivity fails to diverge as $T \rightarrow 0$, dubbed as a “failed insulator.”

In contrast, annealing stage S1 or S2 develops a superconducting ground state in zero field, where the T_c is just below our base temperature for S0 while $T_c \approx 0.4\text{ K}$ for S1. Nev-

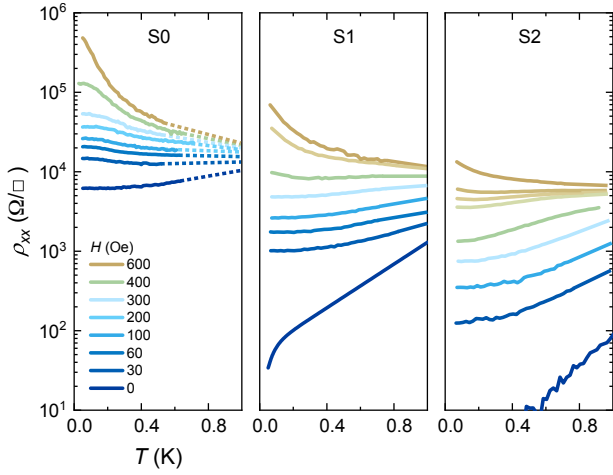


Fig. 3. Temperature dependence of resistivity. $\rho(T)$ in varying magnetic field for three successive annealing stages S0–S2. Dotted lines in S0 connects cooling data < 0.7 K with a field sweep at 1.1 K.

coordination number of the random array of indium grains of average size $\sim 0.1 \mu\text{m}$ (8). Taking a dielectric constant of ~ 10 for the InO_x , and average distance between grains of ~ 10 nm, we obtain E_{aI} in the range that we find experimentally in Fig. 4a. The corresponding $(\sigma_{QF})^{-1}$ increases in the high field limit to order of $\sim 1 \text{ M}\Omega$, emphasizing the fact that this saturated resistance is much larger than the quantum of resistance R_Q .

To quantitatively analyze resistivity saturation on the *superconducting* side, we adopt a similar empirical law by exchanging the role of resistivity ρ and conductivity σ , justified as a manifestation of charge-phase correspondence (or particle-vortex duality) near either a direct SIT or an “avoided” SIT – a crossover between failed superconductors and failed insulators (8, 14).

$$\rho(T) = \rho_{QF} + \rho_0 \cdot \exp(-E_{aS}/k_B T) \quad [2]$$

where ρ_{QF} is an analogous temperature-independent contribution to resistivity and E_{aS} is activation energy on the superconducting side. Fits of this form to resistivity of S1 are shown in Fig. 4b, where Eqn. 1 is used for $H \geq 350$ Oe and Eqn. 2 for $H \leq 300$ Oe. The left y-axis shows ρ_{QF}^{-1} from low field and σ_{QF} from high field in the same plot. Quantum fluctuation contribution ρ_{QF} grows (or equivalently, ρ_{QF}^{-1} shrinks) upon increasing field, while quantum fluctuation contribution σ_{QF} shrinks in higher fields. The field dependence for both branches are power laws with $\rho_{QF}^{-1} \propto H^{-0.45}$ and $\sigma_{QF} \propto H^{-4.7}$. Activation temperature on the low field side is around 1.5 K and gradually decreasing, until a sharp drop at $H^* \sim 300$ Oe where the sample switches to insulating behavior. Besides a factor of ~ 4 difference between activation temperatures in the two regimes, the qualitative trend in field is consistent with those in S0. The dome-shaped presence of ρ_{QF} and σ_{QF} suggests that quantum fluctuations play important roles in both regimes of anomalous metallic phase.

Discussion

The evolution of zero-temperature behaviors of resistivity in S0 and S1 leads us to a holistic understanding of the $T = 0$ phase diagram in Fig. 1. We identify the blue trace (SQMT) as a magnetic-field-tuned (or annealing-tuned) quantum superconductor–anomalous-metal transition (solid line), followed by a transition to an insulating ground state (solid line). The anomalous metallic regime can be further divided into failed-superconductor and failed-insulator regimes, separated by an “avoided” SIT (dash-dot line) representing a wide crossover regime. We also identify the green trace as an annealing-tuned failed-insulator–failed-superconductor transition (QMIT), similar to the magnetic-field controlled scenario despite a fundamental difference in the nature of these two control parameters. As an example, universal anomalous metallic behaviors under different tuning parameter was recently discussed in Ref. (37). Finally, a direct SIT that is typically found in homogeneous films or granular materials with stronger coupling is shown as the red trace (SIT), while transition to a disordered 2D metallic phase appears when Cooper-pairs are broken (dashed line). Within our granular system of In/InO_x composite, a true H-SIT (15) can be tuned to unveil an avoided H-SIT, which was previously shown to exhibit vestiges of self duality around the putative quantum critical point (8). The analysis presented in the previous section explores the duality idea in a wider temperature range which includes the

ertheless, in low field $\lesssim 400$ Oe, the ground state is a failed superconductor and has been discussed extensively (8). For S1 at 400 Oe, the system is right on the insulating side of the transition, yet the resistivity saturates as $T \rightarrow 0$ despite an upturn at ~ 0.2 K. In higher field $\gtrsim 400$ Oe for both S1 and S2, resistivity saturation is substantially reduced and the temperature dependence can be fitted by a logarithmic divergence with a large pre-factor (8). Such logarithmic divergence is in stark contrast with the saturated resistivity in S0. Resistivity of insulators typically have exponential (hopping) or weak granularity-induced divergence persisting to zero-temperature, meaning their curvature $d^2\rho/dT^2$ remains positive as $T \rightarrow 0$. However, in S0 the resistivity divergence is cutoff by a saturation, marked by a sign change in the curvature in the temperature dependence at around 0.2 K (see Fig. 4a).

To quantitatively analyze the evolution of resistivity behavior as a function of magnetic field on the *insulating* side, we adopt an empirical functional form Eqn. 1, which satisfactorily fits S0 data as shown in Fig. 4a. This empirical law was previously employed (13) to describe an analogous conductivity saturation in insulating JJ arrays. The saturation was modeled as a consequence of a temperature-independent quantum fluctuation term σ_{QF} , in addition to thermally-activated conductivity on the insulating side with activation energy E_{aI} and a proportionality constant σ_0 . In writing this equation we assume hall conductivity is zero:

$$\rho(T) = [\sigma_{QF} + \sigma_0 \cdot \exp(-E_{aI}/k_B T)]^{-1} \quad [1]$$

Fig. 4a shows an overlay of the extracted quantum fluctuation contribution σ_{QF} (left axis) and activation temperature E_{aI}/k_B (right axis) as a function of magnetic field. Since σ_{QF} is intimately related to the saturation, it decreases as field increases until around 600 Oe, where the divergence is restored and the saturation disappears. Meanwhile, the activation temperature starts off at around 0.3 K, peaks at just below 0.6 K near 300 Oe, and subsequently decreases before leveling off at high fields. Since the overall tendency for an insulating behavior is governed by the charging energy, we may estimate $E_{aI} \approx \alpha E_C$, where $\alpha \approx 1/\langle z \rangle$ and $\langle z \rangle \approx 6$ is the average

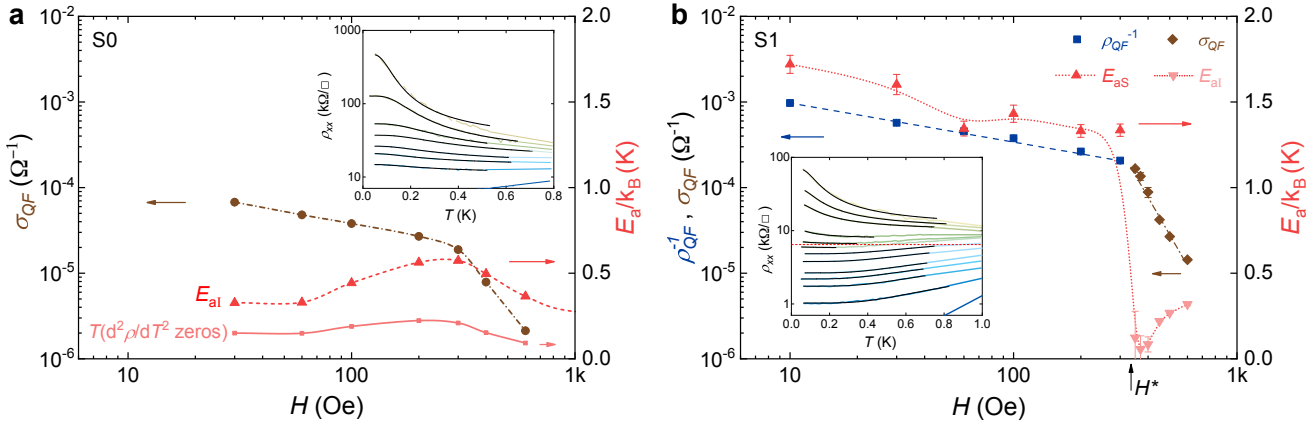


Fig. 4. Evolution of resistivity saturation in magnetic field. **a)** Temperature-independent term σ_{QF} (left axis) and activation temperature E_a/k_B (right axis) extracted from the fits. Also shown are the zeros (light red) in the curvatures of $\rho(T)$. Inset: Temperature dependence of resistivity in S0 fitted by empirical law Eqn. 1. **b)** Temperature-independent term ρ_{QF}^{-1} (■) or σ_{QF} (◆) (left axis) and activation temperature E_a/k_B (right axis) extracted from the fits. Inset: Temperature dependence of resistivity in S1 fitted by empirical laws Eqn. 2. for $H \leq H^*$ and Eqn. 1. for $H \geq H^*$. Also shown is Cooper pair quantum of resistance $R_Q = h/4e^2 \sim 6.5 \text{ k}\Omega/\square$ as the red separatrix. Dotted and dashed lines are guidance to the eye.

resistance saturation associated with the AMS, thus providing further insight into the possible origin of this enigmatic phase. The fact that the data shows a continuous evolution from an AMS with very low sheet resistance to one with very large sheet resistance that far exceeds even the fermion quantum of resistance, h/e^2 , suggests that the superconducting grains and the intergrain tunneling play the key role in determining the saturation value, that is, $(\sigma_{QF})^{-1}$ in Eqn. 1 smoothly connects to ρ_{QF} in Eqn. 2. Focusing on Fig. 4b, it shows that the separating saturation resistance between the two regimes is $\sim 6.5 \text{ k}\Omega/\square$ at the field of $H^* \approx 300 \text{ Oe}$ where the curves change character as a result of the avoided H-SIT. The drop in activation energy between $|E_a|_{H \leq H^*}$ and $|E_a|_{H \gg H^*}$ is a factor of 4. Since H^* marks an avoided transition where we expect $E_J \sim E_C$, then we conclude that E_{aI} saturates to $\frac{1}{4}E_C$ as was previously observed for ordered arrays of JJ (13, 38). This further suggests that for $H \gg H^*$ the saturation is associated with charge fluctuations. Examination of the samples in the reverse direction of annealing (S2 to S1 to S0), we suggest that we observe a smooth crossover of macroscopic quantum effect from a regime dominated by Josephson coupling to a regime dominated by Coulomb interaction, which for each realization of coupling (annealing) and magnetic field could be attributed to a single junction behavior in the respective regime.

Starting from a single resistively-capacitively-shunted-JJ with $E_J \gg E_C$, for a small bias current a phase difference is established along the junction resulting in a zero-voltage supercurrent. However, at very low temperatures where activation is exponentially small, quantum fluctuations of the phase induce quantum tunneling of the phase variable (39) and thus a finite voltage (40, 41). With increasing charging energy, and in the limit $E_J \ll E_C$, a dual situation is expected, where the electric charge on the junction capacitance, which conjugates to the junction's phase, results in Coulomb blockade and thus an insulating state. For a small bias voltage, quantum fluctuations of the charge may give rise to a coherent current of cooper pairs and to dissipation due to single electron tunneling (42). The latter is also a macroscopic quantum effect due

to the participation of the collective electron system in the process (43, 44).

To rationalize the analogy with a single resistively-capacitively-shunted-JJ we follow Fisher (45) assuming that junctions in the $E_J \gg E_C$ regime (Samples S2 and S1) are resistively shunted with a wide distribution of shunt resistors. While in general the idea of a normal conductance channel was challenged in the limit of $T \ll T_c$ for an ordered array of JJs (46), we believe that it is natural to expect normal regions in a random array of grains such as in our In/InO_x composite, especially in the presence of magnetic field (8, 15). Using an Ambegaokar-Halperin-Langer (AHL) approach (47), we assume that there exists a set of junctions which are coupled to shunt resistors large enough to allow phase slips and are connected to form an infinite network that spans the system. By the nature of the effect where the phase slips span the size of the sample for a magnetic field $H_{SM} \ll H_c^*$, we can map it on a random-resistor network (RRN) percolation problem, which at very low temperature, for a given tuning parameter (here the magnetic field) is self-organized to be at criticality. Note that as such, our approach is fully quantum mechanical in a similar way that AHL describes variable range hoping on the insulating side of Anderson localization (see e.g. (48)). A well known result for percolation theory is that the resistance above percolation is bounded from below by the total resistance of the so-called “singly connected bonds” (49–51), that is, the bonds that if cut will disrupt the integrity of the infinite network. Near criticality, for a system of size L , the average conductance is given by $\langle G \rangle = L^{d-1} \langle g_1 \rangle$, where d is the dimensionality and g_1 is the linear conductance of the chain of singly connected bonds estimated here as $\langle g_1 \rangle \sim 1/Lr_s$, where r_s is the limiting shunt resistance (52). In two-dimensions, the value of the saturated resistivity within this RRN-percolation model is easily estimated as $\rho_s \approx \langle G \rangle^{-1} \approx r_s$. Thus, the regime of anomalous metal is a consequence of MQT through junctions characterized by $r_s \ll R_Q$.

Turning to the more insulating samples (S0, and high-field S1), the intergrain mediating InO_x layer is insulating enough

301 (single junction resistance $\gg R_Q$) to prevent an infinite cluster
 302 of percolating phase-coherent superconducting grains even at
 303 zero magnetic field. At a finite field, $E_C/E_J \gg 1$, and with
 304 mesoscopic fluctuations in local conductance, dissipation may
 305 arise from a shunt resistor, or discrete tunneling of quasiparticles
 306 and shot noise, irrespective of the otherwise macroscopic
 307 effect of localization in the 2D InOx system (42). In this
 308 regime, the small grains, which appear interstitially between
 309 the larger superconducting islands, become the bottleneck for
 310 continuous conduction due to their large charging energy sat-
 311 isfying $E_C \gg E_J$. This situation is amplified with increasing
 312 magnetic field where more of the weaker junctions between
 313 large superconducting islands lose phase coherence. At the
 314 same time, a true insulating state as a consequence of Coulomb
 315 blockade may fail because of MQT of charge (13, 44). This
 316 dual behavior to the phase-MQT suggests to extend the per-
 317 colation description according to Ambegaokar, Halperin and
 318 Langer results (47) to the insulating side where a saturated
 319 resistivity is expected with limiting junction shunt resistance
 320 $r_s \gg R_Q$ and $E_C \gg E_J$.

321 The phase-charge duality is further understood by the in-
 322trinsic duality of the RRN of the randomly distributed shunt
 323 resistances underlying the JJ array. Indeed, there is an exact
 324 relation between the bulk effective conductivity of a 2D con-
 325 tinuous composite made of two isotropic components and that
 326 of the dual composite (51, 53–57). For a rectangular array of
 327 JJ representing bonds with resistances $\{r_i\}$ and conductances
 328 $\{g_i\}$ (where $g_i^D = 1/r_i \equiv r_i$), the dual total conductance
 329 $G_x^D(g_1^D, g_2^D, \dots, g_N^D)$ along x -direction is related to the con-
 330 ductance along the y -direction $G_y(g_1, g_2, \dots, g_N) \equiv R_y(r_1, r_2, \dots, r_N)$
 331 as: $G_x^D = 1/G_y$. The same average behavior is expected
 332 for the random system, which is manifested in our random
 333 In/InO_x composite (51, 53, 54): $\langle G_x^D \rangle = \langle R_y \rangle$. The charge-
 334 phase correspondence maps onto the RRN duality and further
 335 reinforces the vestiges of duality that originate from the H-SIT
 336 as previously suggested by Shimshoni *et al.*, (22).

337 A further consequence of the above model is the realization
 338 of the fragility of the superconducting or insulating states from
 339 which the failed superconductor and failed insulator emerge.
 340 Besides the annealing and magnetic field, any perturbation
 341 applied to the system strongly affects the distribution of junc-
 342 tions properties, thus leading to a shift in the potential barrier
 343 for the MQT process resulting in a shift of the saturated resis-
 344 tance. For example, external radiation can work to enhance
 345 the quantum fluctuations and thus AMS will emerge with
 346 larger saturated resistance as $T \rightarrow 0$ (20), or reduce them and
 347 thus pin the superconducting state (8). Similarly, a ground
 348 plane near a sample can provide another dissipation channel
 349 to pin the superconducting state, as well as alter the charging
 350 energies to modify the saturation on the insulating side, both
 351 effects were observed in JJ arrays (58) and in highly disordered
 352 films (59).

353 In summary, we identify two regimes in anomalous metallic
 354 phase – a “failed superconductor” and a “failed insulator,” as
 355 clearly suggested by resistivity saturation on both sides of
 356 an “avoided” SIT. The close connection between our granular
 357 composite and Josephson junction arrays is revealed by a set
 358 of empirical fits to the temperature dependence of resistivity.
 359 Quantum fluctuations of phase drive the transition from
 360 superconductor to anomalous metal when superconductors
 361 fail to establish global phase coherence, while quantum fluc-

tuations of charge number drive the transition from insulator
 362 to anomalous metal when charge localization gives way to
 363 dissipative transport. A duality picture is strongly justified
 364 in our discussions by interchanging the roles of N and ϕ and
 365 corroborated by the resemblance of transport behaviors when
 366 exchanging the roles of ρ and σ .
 367

Materials and Methods

InO_x/In granular composites were grown by electron-beam evap-
 368 oration of In₂O₃ in oxygen partial pressure, followed by that of
 369 In under high vacuum. Consecutive *in situ* depositions of the two
 370 components result in a clean interface that is crucial for optimal
 371 interface coupling. The uniform underlying amorphous InO_x is
 372 specifically prepared to be weakly insulating to mediate couplings
 373 among the In grains and nearby proximitized regions. Details of
 374 the sample preparation process were provided in Ref. (8).
 375

376 Resistivity was measured on a patterned hall-bar sample using
 377 standard four-point lock-in technique. Current excitation was pro-
 378 vided by reference ac voltage source in series with a 1-GΩ resistor
 379 that is much more resistive than any measured sample resistance
 380 in this study. The current intensity ranged from 0.1 nA to 1 nA
 381 while the frequency varied between 0.7–7 Hz depending on sample
 382 resistance. Linear response to excitation current was confirmed at
 383 the highest resistance. Temperature ramps were sufficiently slow
 384 compared to the prolonged time constant.
 385

386 In our dilution refrigerator, all measurement wires were filtered
 387 at both room temperature and mixing chamber temperature ($T \gtrsim$
 388 10 mK) using commercial in-line pi-filters and cryogenic filters,
 389 achieving over 100 dB attenuation throughout 100 MHz–5 GHz
 390 range. Sample phonon temperature was measured by a calibrated
 391 on-chip RuO₂ thermometer subject to the same mounting and
 392 wiring as the sample. Data is not considered in our analysis when
 393 sample temperature differs more than 10% from mixing chamber
 394 temperature. The refrigerator was operating at the highest cooling
 395 power with an extra circulation pump running, despite at the cost
 396 of a higher base (mixing chamber) temperature.
 397

ACKNOWLEDGMENTS. We acknowledge discussions with Steven
 398 Kivelson, Sri Raghu, Boris Spivak, and Yacov Kantor. Work at
 399 Stanford University was supported by the National Science Foundation
 400 Grant NSF-DMR-1808385. Work at Tel-Aviv University was
 401 supported by the US-Israel Binational Science Foundation (Grant
 402 No. 2014098). We thank Sejoon Lim for assistance with SEM. Part
 403 of this work was performed at the Stanford Nano Shared Facilities
 404 (SNSF), supported by the National Science Foundation under award
 405 ECCS-1542152.
 406

1. Ephron D, Yazdani A, Kapitulnik A, Beasley MR (1996) Observation of quantum dissipation in the vortex state of a highly disordered superconducting thin film. *Phys. Rev. Lett.* 76(9):1529–1532.
 407
2. Chen CD, Delsing P, Haviland DB, Harada Y, Claeson T (1996) Flux flow and vortex tunneling in two-dimensional arrays of small Josephson junctions. *Phys. Rev. B* 54(13):9449–9457.
 408
3. Mason N, Kapitulnik A (1999) Dissipation effects on the superconductor-insulator transition in 2d superconductors. *Phys. Rev. Lett.* 82(26):5341–5344.
 409
4. Breznay NP, Kapitulnik A (2017) Particle-hole symmetry reveals failed superconductivity in the metallic phase of two-dimensional superconducting films. *Science Advances* 3(9):e1700612.
 410
5. Böttcher CGL, et al. (2018) Superconducting, insulating and anomalous metallic regimes in a gated two-dimensional semiconductor-superconductor array. *Nature Physics* 14(11):1138–1144.
 411
6. Chen Z, et al. (2018) Carrier density and disorder tuned superconductor-metal transition in a two-dimensional electron system. *Nature Communications* 9(1):4008.
 412
7. Yang C, et al. (2019) Intermediate bosonic metallic state in the superconductor-insulator transition. *Science* 366:6472.
 413
8. Zhang X, Hen B, Palevski A, Kapitulnik A (2021) Robust anomalous metallic states and vestiges of self-duality in two-dimensional granular In-InO_x composites. *npj Quantum Mater.* 6:30.
 414
9. Kapitulnik A, Kivelson SA, Spivak B (2019) Colloquium: Anomalous metals: Failed superconductors. *Rev. Mod. Phys.* 91(1):011002.
 415
10. Mason N, Kapitulnik A (2001) True superconductivity in a two-dimensional superconducting insulating system. *Phys. Rev. B* 64(6):060504(R).
 416
11. Jaeger HM, Haviland DB, Goldman AM, Orr BG (1986) Threshold for superconductivity in ultrathin amorphous gallium films. *Phys. Rev. B* 34(7):4920–4923.
 417
12. Couédo F, et al. (2016) Dissipative phases across the superconductor-to-insulator transition. *Scientific Reports* 6(1):35834.
 418

433 13. Delsing P, Chen CD, Haviland DB, Harada Y, Claeson T (1994) Charge solitons and quantum
434 fluctuations in two-dimensional arrays of small josephson junctions. *Phys. Rev. B* 50(50):3959–
435 3971.

436 14. Breznay NP, Steiner MA, Kivelson SA, Kapitulnik A (2016) Self-duality and a hall-insulator
437 phase near the superconductor-to-insulator transition in indium-oxide films. *Proc. Natl. Acad.
438 Sci. U.S.A.* 113(2):280–285.

439 15. Hen B, Zhang X, Shelukhin V, Kapitulnik A, Palevski A (2021) Superconductor-insulator
440 transition in two-dimensional indium-indium-oxide composite. *Proceedings of the National
441 Academy of Sciences* 118(2):e2015970118.

442 16. Spivak B, Zyzin A, Hruska M (2001) Quantum superconductor-metal transition. *Phys. Rev. B*
443 64(13):132502.

444 17. Spivak B, Oreo P, Kivelson SA (2008) Theory of quantum metal to superconductor transitions
445 in highly conducting systems. *Phys. Rev. B* 77(21):214523.

446 18. Averin DV, Likharev KK (1986) Coulomb blockade of single-electron tunneling, and coherent
447 oscillations in small tunnel junctions. *Journal of Low Temperature Physics* 62(3):345–373.

448 19. Fazio R, Schön G (1991) Charge and vortex dynamics in arrays of tunnel junctions. *Phys. Rev.
449 B* 43(7):5307.

450 20. Tamir I, et al. (2019) Sensitivity of the superconducting state in thin films. *Science Advances*
451 5(3):eaau3826.

452 21. Mulligan M, Raghu S (2016) Composite fermions and the field-tuned superconductor-insulator
453 transition. *Phys. Rev. B* 93(20):205116.

454 22. Shimshoni E, Auerbach A, Kapitulnik A (1998) Transport through quantum melts. *Phys. Rev.
455 Lett.* 80(15):3352–3355.

456 23. Ghosal A, Randeria M, Trivedi N (1998) Role of spatial amplitude fluctuations in highly
457 disordered s-wave superconductors. *Phys. Rev. Lett.* 81(18):3940–3943.

458 24. Skvortsov MA, Feigel'man MV (2005) Superconductivity in disordered thin films: Giant meso-
459scopic fluctuations. *Phys. Rev. Lett.* 95(5):057002.

460 25. Dubi Y, Meir Y, Avishai Y (2007) Nature of the superconductor-insulator transition in disordered
461 superconductors. *Nature* 449(7164):876–880.

462 26. Müller M, Shklovskii BI (2009) Compensation-driven superconductor-insulator transition. *Phys.
463 Rev. B* 79(13):134504.

464 27. Feigel'man MV, Larkin AI (1998) Quantum superconductor-metal transition in a 2d proximity-
465 coupled array. *Chemical Physics* 235(1):107–114.

466 28. Kapitulnik A, Deutscher G (1984) Comments on computer investigations of micrographs of
467 metal films near their continuity threshold. *Thin Solid Films* 113:79–84.

468 29. Mühlischlegel B, Scalapino DJ, Denton R (1972) Thermodynamic properties of small super-
469 conducting particles. *Phys. Rev. B* 6(5):1767.

470 30. Entin-Wohlman O, Kapitulnik A, Shapira Y (1981) Dependence of T_c on the normal-state
471 resistivity in granular superconductors. *Phys. Rev. B* 24(11):6464.

472 31. Ioffe LB, Larkin AI (1981) Properties of superconductors with a smeared transition temperature.
473 *Zh. Éksp. Teor. Fiz.* 81(2):707. [Sov. Phys. JETP **54**, 378 (1981)].

474 32. Imry Y, Strongin M (1981) Destruction of superconductivity in granular and highly disordered
475 metals. *Phys. Rev. B* 24(11):6353.

476 33. Merchant L, Ostrick J, Barber RP, Dynes RC (2001) Crossover from phase fluctuation to
477 amplitude-dominated superconductivity: A model system. *Phys. Rev. B* 63(13):134508.

478 34. Abeles B (1977) Effect of charging energy on superconductivity in granular metal films. *Phys.
479 Rev. B* 15(5):2828–2829.

480 35. Efetov KB (1980) Phase transition in granulated superconductors. *Zh. Éksp. Teor. Fiz.*
481 78(5):2017. [Sov. Phys. JETP **51**, 1015 (1980)].

482 36. Koval D, Ovadyahu Z (1994) Disorder induced granularity in an amorphous superconductor.
483 *Solid State Commun.* 90(12):783.

484 37. Chen Z, et al. (2021) Universal behavior of the bosonic metallic ground state in a two-
485 dimensional superconductor. *npj Quantum Mater.* 6:15.

486 38. Tighe TS, Tuominen MT, Hergenrother JM, Tinkham M (1993) Measurements of charge
487 soliton motion in two-dimensional arrays of ultrasmall josephson junctions. *Phys. Rev. B*
488 47(2):1145–1148.

489 39. Caldeira A, Leggett A (1983) Quantum tunnelling in a dissipative system. *Annals of Physics*
490 149(2):374–456.

491 40. Schwartz DB, Sen B, Archie CN, Lukens JE (1985) Quantitative study of the effect of the
492 environment on macroscopic quantum tunneling. *Phys. Rev. Lett.* 55(15):1547–1550.

493 41. Martinis JM, Devoret MH, Clarke J (1987) Experimental tests for the quantum behavior of a
494 macroscopic degree of freedom: The phase difference across a josephson junction. *Phys.
495 Rev. B* 35(10):4682–4698.

496 42. Schön G, Zaikin A (1990) Quantum coherent effects, phase transitions, and the dissipative
497 dynamics of ultra small tunnel junctions. *Physics Reports* 198(5):237–412.

498 43. Iansiti M, et al. (1987) Charging energy and phase delocalization in single very small josephson
499 tunnel junctions. *Phys. Rev. Lett.* 59(4):489.

500 44. Geerligs LJ, Averin DV, Mooij JE (1990) Observation of macroscopic quantum tunneling
501 through the coulomb energy barrier. *Phys. Rev. Lett.* 65(24):3037–3040.

502 45. Fisher MPA (1986) Quantum phase slips and superconductivity in granular films. *Phys. Rev.
503 Lett.* 57(7):885–888.

504 46. Chakravarty S, Kivelson S, Zimanyi GT, Halperin BI (1987) Effect of quasiparticle tunneling on
505 quantum-phase fluctuations and the onset of superconductivity in granular films. *Phys. Rev. B*
506 35(13):7256–7259.

507 47. Ambegaokar V, Halperin BI, Langer JS (1971) Hopping conductivity in disordered systems.
508 *Phys. Rev. B* 4(8):2612–2620.

509 48. Mott NF, Pepper M, Pollitt S, Wallis RH, J. AC (1975) The anderson transition. *Proc. R. Soc.
510 Lond. A* 345(1641):169–205.

511 49. Coniglio A (1981) Thermal phase transition of the dilute s-state potts and n-vector models at
512 the percolation threshold. *Phys. Rev. Lett.* 46(4):250–253.

513 50. Coniglio A (1982) Thermal phase transition of the dilute s-state potts and n-vector models at
514 the percolation threshold. *J. Phys. A: Math. Gen.* 15(12):3829.

515 51. Wright DC, Bergman DJ, Kantor Y (1986) Resistance fluctuations in random resistor networks
516 above and below the percolation threshold. *Phys. Rev. B* 33(1):396–401.